# Reflectance analysis for 3D computer graphics model generation

Yoichi Sato and Katsushi Ikeuchi

June 11, 1995

CMU-CS-95-146

School of Computer Science
Carnegie Mellon University
Pittsburgh, Pennsylvania 15213-3890

This research was sponsored in part by the Advanced Research Projects Agency under the Department of the Army, Army Research Office under grant number DAAH04-94-G-0006, partially by NSF under Contract IRI-9224521, and in part by the Advanced Research Projects Agency under the U.S. Air Force, the Avionics Laboratory, Wright Research and Development Center, Aeronautical Systems Division (AFSC), Wright-Patterson AFB under Contract F33615-90-C-1465, ARPA Order No. 7597.

**Keywords**: Computer vision, computer graphics, three dimensional model measurement, color reflectance analysis.

## Abstract

For synthesizing realistic images of a real three dimensional object, reflectance properties of the object surface, as well as the object shape, need to be measured. This paper describes one approach to create a three dimensional object model with physically correct reflectance properties by observing a real object. The approach consists of three steps. First, a sequence of range images and color images is measured by rotating a real object on a rotary table with fixed viewing and illumination directions. Then, the object shape is obtained as a collection of triangular patches by merging multiple range images. Secondly, by using the recovered object shape, color pixel intensities of the color image sequence are separated into the diffuse reflection component and the specular reflection component. Finally, the separated reflection components are used to estimate parameters of the Lambertian reflection model and a simplified Torrance-Sparrow reflection model. We have successfully tested our approach by using images of a real object. Synthesized images of the object under arbitrary illumination conditions are shown in this paper.

# 1 Introduction

Recently, a demand for highly realistic synthesized images has been expanding rapidly in many applications such as virtual reality and electrical museums. For generating realistic images of a three dimensional object, two aspects of information are fundamental: the object's shape and reflectance properties such as color and specularity. We call those two aspects of information the geometric information and the photometric information. Significant improvements have been achieved in the field of computer graphics hardwares and image rendering algorithms. However, it is often the case that three dimensional models are created manually by users. That input process is normally time-consuming and can be a bottle neck for realistic image synthesis. Therefore, techniques to obtain object model data automatically by observing a real object could have great significance in practical applications.

Techniques for measuring the geometric information by using range data from real objects have been intensively studied in the past. Turk and Levoy developed a system which can merge multiple surface meshes one by one, by using two step strategy: registration by the iterative closest point algorithm (ICP algorithm) and integration by the zippering algorithm [23]. Higuchi and Ikeuchi has developed a method for merging multiple range views of a free-form surface obtained from arbitrary viewing directions, with no initial estimation of relative transformation among those viewing directions [6]. The method is based on the Spherical Attribute Image (SAI) representation of free-form surfaces which was originally introduced by Delingette, Hebert and Ikeuchi in [4]. Hoppe, DeRose, and Duchamp [7] have introduced an algorithm to construct three dimensional surface models from a cloud of points without spatial connectivity. The algorithm differs from others in that it does not require surface meshes as input. It is important to see that those techniques are mainly focused on obtaining the geometric information from range data, but only limited attention has been paid to the photometric information such as reflectance properties.

On the other hand, techniques to obtain the geometric information and the photometric information only from intensity images have been developed by other researchers. Sato and Ikeuchi [18] introduced a method to analyze a sequence of color images taken under a moving light source. They successfully estimated parameters of a reflectance function as well as object shapes, by explicitly separate the diffuse and specular reflection components. Subsequently, the technique has been applied to analyze a color image sequence taken in an outdoor environment under solar illumination [19]. Lu and Little developed a method to estimate a reflectance function from a sequence of black and white images of a rotating smooth object, and the object shape was successfully recovered by using the estimated reflectance function [12]. Since the reflectance function is measured directly from the input image sequence, the method does not assume a particular reflection model such as the Lambertian model which is commonly used in computer vision. However, the method works only for smooth objects which are symmetric about a rotation axis. Another interesting attempt for measuring a reflectance function from intensity images has been reported by Ward [24]. Ward designed a special device with a half-silvered hemisphere and a CCD video camera, which can measure a bidirectional reflectance distribution function (BDRF) of anisotoropic reflection. The main advantage of the device is that it takes significantly less time to measure a BDRF than a conventional gonioreflectometer. A BDRF of a real object surface has been measured by the device and highly realistic images are synthesized. However, this approach cannot be easily extended for modeling real object with various reflectance properties. A small piece of test material has to be given to measure the material's BDRF. In addition, an object shape was not measured and simply given by a user manually.

Recently, techniques to measure the geometric and photometric information together by using both range images and black and white intensity images have been studied. Ikeuchi and Sato originally developed a method to measure object shapes and reflection function parameters from one set of range image and intensity image [9]. In their attempt, the surface shape is recovered from the range image at first, and then surface normals of the recovered object surface are used for reflectance parameter estimation. The main drawback of the method is that it assumes uniform reflectance properties over the object surface. Additionally, only partial object shape was recovered because only one range image was used. Kay and Caelli introduced another method to use a set of a range image and 4 or 8 intensity images taken under different illumination conditions [10]. By increasing the number of intensity images, they estimated reflection function parameters locally for each image pixels. Unlike the algorithm proposed by Sato and Ikeuchi, the method can handle object surfaces with varying reflectance properties. However, it is reported that parameter estimation can be unstable especially when the specular reflection component is not observed strongly.

In this paper, we propose one approach to recover both the geometric and photometric information from a sequence of range images and color images of a rotating object. Unlike previously introduced methods, our approach is cable of estimating parameters of a reflection function locally in a robust manner. Firstly, a sequence of range images is used for recovering an entire shape of the object as a collection of triangular patches. The zipper system developed by Turk and Levoy [23] is used for the shape recovery stage. Then, a sequence of color images are mapped onto the recovered shape. As a result, we can determine observed color changes through the image sequence for all triangular patches of the object surface. The observed color sequence is separated into the diffuse reflection component and the specular reflection component by the algorithm used originally by Sato and Ikeuchi in [18]. Subsequently, parameters of a reflection function used in our analysis are estimated reliably for the diffuse and specular reflection components. The reflection model used here is described as a linear combination of the Lambertian model and the Torrance-Sparrow model The Torrance-Sparrow model is modified according to our experimental setup where the viewing and illumination directions are always the same. Finally, color images of the object are synthesized from the recovered shape and reflectance properties to demonstrate the feasibility of the proposed approach.

The paper is organized as follows. The section 2.1 describes the recovery of an object shape from a sequence of range images. In the section 2.2, a projection of color images onto the recovered object shape will be explained. The section 3.1 introduces the reflection model used in our experiment. The algorithm for separating the diffuse and specular reflection components is explained in the section 3.2, and reflectance parameter estimation is discussed in the section 3.3. The algorithm is applied to range images and color images of a real object, and experimental results will be shown in the section 4. Concluding remarks are presented in the section 5.

# 2 Modeling of geometric information

## 2.1 Shape recovery

In this section, a method for generating a three dimensional object shape from multiple range images is described.

In the past, there have been a large number of techniques investigated for constructing three dimensional object shapes from unorganized or organized points. For instance, Turk and Levoy [23] developed a technique to combine multiple range images one by one, using a two step strategy: registration and integration. Their technique uses a modified version of the iterated closest-point algorithm (ICP algorithm) which was originally developed by Besl and McKay [2]. After the registration procedure, two surface meshes composed of small triangular patches are integrated to produce one combined surface mesh. They called the integration algorithm *the zipper algorithm*. Turk and Levoy's zipper algorithm is effective for producing an object model with a large number of triangular patches. In their paper [2], example objects typically consist of over 100,000 triangle patches. One of the advantages of the zipper system is that it does not require an accurate relative transformation between the range images. That is because the all range images can be aligned by using the ICP algorithm. We found that it is still advantageous even when the relative transformation can be measured directly (e.g. using a rotary table). The zipper system takes surface meshes created from range images as its input. That reduces the complexity of the integration algorithm significantly, while other algorithms use a collection of data points without connectivity information among the points. Because of the zipper system's advantages mentioned here, we decided to use the system for modeling geometric information of real objects. For more details of the zipper system, refer to the paper by Turk and Levoy [23].

Range images are obtained by using a light stripe range finder with a liquid crystal shutter and a color CCD video camera [17]. It can compute three dimensional point locations corresponding to image pixels based on optical triangulation. For each range image, a set of six images is obtained. Those images contain x, y and z locations and red, green, and blue color band values of all pixels. Pixels of the range images and the color images correspond because all images are captured by using the same camera. An experimental setup used in our experiments is illustrated in Figure 1. A single point light source is used for illuminating a target object. The light source is located nearby the camera lens, so that both the viewing direction and the illumination direction are approximately the same.

First, the range finder is calibrated by using a calibration box of known size and shape. The calibration produces a $4 \times 3$ matrix which represents the projection transformation between the world coordinate system and the image coordinate system. The projection transformation matrix will be used for mapping a sequence of input color images onto the recovered object shape (section 2.2). An object whose shape and reflectance information are to be recovered is located on a computer-controlled rotary table. Then, range and color images are captured by the range finder at a fixed angle step of object orientation. Each range image is used for creating a surface mesh which consists of small triangular patches. Following the measurement of range and color images, the zipper system is used for combining all surface meshes to create a merged object shape. The recovered object shape and a sequence of input color images will be used for analyzing the object's reflectance properties later, which will be explained in the section 3.

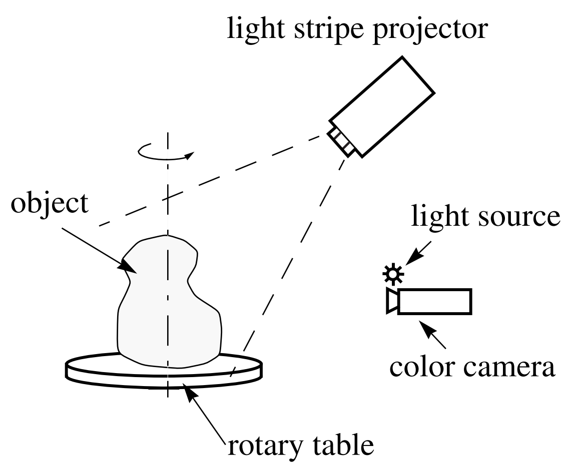


**Figure 1 Experimental setup**

## 2.2 Mapping color images onto recovered object shape

The recovered object shape and the sequence of input color images are used for estimating reflection model parameters at each triangular patch. The algorithm to estimate reflectance parameters of the object surface from the sequence of color images will be explained in the section 3.

For the reflectance parameter estimation, we need to know how the observed color changes at each triangular patch, as the object rotates. That can be done by mapping the sequence of color images onto the recovered object shape. The recovered object shape as a collection of triangular patches is defined in a three dimensional world coordinate system. The rotary table's location and orientation in the world coordinate system are given by calibration. Thus, locations of all triangular patches in the world coordinate system can be easily computed for each orientation of the object. Subsequently, the triangular patches are projected back onto the image plane by using the $4 \times 3$ projection transformation matrix based on a perspective projection model. The center of the projection is simply computed from the projection matrix [21]. The Z-buffer algorithm is used for determining visible triangular patches and their locations on the image plane.

Ideally, all triangular patches are small enough to have uniform color on the image plane. However, a projection of a triangular patch on the image plane often corresponds to multiple image pixels of different color. Therefore, the average color intensity of all corresponding pixels is assigned to the triangular patch. It would be a straightforward extension to assign a two dimensional array to each triangular patch to store all pixel colors when the resolution of triangular patches is high enough.

By applying the procedure explained above for all object orientations, we finally get a collection of triangular patches each of which has a sequence of observed color with respect to the object orientation.

# 3 Modeling of photometric information

## 3.1 Reflection model

In this section, a reflectance model used in this report is described. The reflectance model will be used later for separating the diffuse and surface reflection components from a sequence of color images. The reflection component separation will be described in the section 3.2. The model will also be used for reflectance parameter estimation which will be explained in the section 3.3.

A mechanism of reflection is described in terms of three reflection components, namely the diffuse lobe, the specular lobe, and the specular spike [13]. The diffuse lobe component is explained as internal scattering. When an incident light ray penetrates object surface, it is reflected and refracted repeatedly at a boundary between small particles and medium of the object. The scattered light ray eventually reaches the object surface, and is refracted into the air in various directions. This phenomenon results in the diffuse lobe component. The Lambertian model is based on the assumption that those directions are evenly distributed in all directions. In this paper, the Lambertian model is used for modelling the diffuse lobe component.

Unlike the diffuse lobe and the specular lobe components, the specular spike component is not commonly observed in many actual applications. The component can be observed only from mirror-like smooth surfaces where reflected light rays of the specular spike component are concentrated in a specular direction. That makes it hard to observe the specular spike component from viewing directions at coarse sampling angles. Therefore, in many computer vision and computer graphics applications, a reflection mechanism is modelled as a linear combination of two reflection components: the diffuse lobe component and the specular lobe component. Those two reflection components are normally called the diffuse reflection component and the specular reflection component, respectively. The reflection model was formally introduced by Shafer as the dichromatic reflection model [20]. Based on the dichromatic reflection model, the reflection model used in our analysis is represented as a linear combination of the diffuse reflection component and the specular reflection component. The Lambertian model and the Torrance-Sparrow model are used for modelling those two reflection components, respectively. As Figure 1 illustrates, illumination and viewing directions are fixed and the same. In Appendices of this paper, the reflection model used for the particular experiment setup is derived and given as:

$$I_m = K_{diff,m}\cos\theta + K_{spec,m}\frac{1}{\cos\theta}e^{-\frac{\theta^2}{2\sigma_\alpha^2}} \qquad m = red, green, blue \tag{EQ1}$$

where $\theta$ is the angle between the surface normal and the viewing direction (or the light source direction) (Figure 10), $K_{diff,m}$ and $K_{surf,m}$ are a constant for each reflection component, $\sigma_\alpha$

is the standard deviation of a facet slope $\alpha$ of the Torrance and Sparrow model. The direction of the light source and the camera with respect to the surface normal is referred as the sensor direction $\theta$ in this paper.

## 3.2 Reflection component separation

The algorithm to separate the two reflection components is described here. The separation of the two fundamental reflection components is important for robust estimation of reflectance parameters. It has been reported that estimating all reflectance parameters at once tends to make computation unstable and sometimes makes it hard to converge [10]. Therefore, the separation algorithm is applied prior to reflectance parameter estimation. The separation algorithm was originally introduced for the case of a moving light source by Sato and Ikeuchi in [18]. In this paper, a similar algorithm is applied for the case of a moving object.

Using three color bands: red, green, and blue, the coefficients $K_{diff,\,m}$ and $K_{spec,\,m}$, in (EQ1), become two linearly independent vectors, $\underset{\sim}{K}_{diff}$ and $\underset{\sim}{K}_{spec}$, unless the colors of the two reflection components are accidentally the same:

$$\underset{\sim}{K}_{diff} = \begin{bmatrix} K_{diff,\,red} \\ K_{diff,\,green} \\ K_{diff,\,blue} \end{bmatrix} = \begin{bmatrix} g\int_{\lambda} \tau_{\mathrm{red}}(\lambda)\, k_{\mathrm{diff}}(\lambda)\, s(\lambda)\, d\lambda \\ g\int_{\lambda} \tau_{\mathrm{green}}(\lambda)\, k_{\mathrm{diff}}(\lambda)\, s(\lambda)\, d\lambda \\ g\int_{\lambda} \tau_{\mathrm{blue}}(\lambda)\, k_{\mathrm{diff}}(\lambda)\, s(\lambda)\, d\lambda \end{bmatrix} \qquad \textbf{(EQ2)}$$

$$\underset{\sim}{K}_{spec} = \begin{bmatrix} K_{spec,\,red} \\ K_{spec,\,green} \\ K_{spec,\,blue} \end{bmatrix} = \begin{bmatrix} g\int_{\lambda} \tau_{\mathrm{red}}(\lambda)\, k_{\mathrm{spec}}(\lambda)\, s(\lambda)\, d\lambda \\ g\int_{\lambda} \tau_{\mathrm{green}}(\lambda)\, k_{\mathrm{spec}}(\lambda)\, s(\lambda)\, d\lambda \\ g\int_{\lambda} \tau_{\mathrm{blue}}(\lambda)\, k_{\mathrm{spec}}(\lambda)\, s(\lambda)\, d\lambda \end{bmatrix} \qquad \textbf{(EQ3)}$$

These two vectors represent the colors of the diffuse and specular reflection components in the dichromatic reflectance model [20].

First, the observed color intensities in the R, G, and B channels with $n$ different object orientations, are measured at each triangular patch of the recovered object shape. It is important to note that all intensities are measured *at the same triangular patch*. The three sequences of intensity values are stored in the columns of an $n \times 3$ matrix $M$. Considering the reflectance model and two color vectors in (EQ1), (EQ2), and (EQ3), the intensity values in the R, G, and B channels can be represented as:

$$
\begin{aligned}
M &= \begin{bmatrix} \underset{\sim}{M}_R & \underset{\sim}{M}_G & \underset{\sim}{M}_B \end{bmatrix} \\
&= \begin{bmatrix} \cos\theta_1 & P(\theta_1) \\ \cos\theta_2 & P(\theta_2) \\ \cdot & \cdot \\ \cdot & \cdot \\ \cos\theta_n & P(\theta_n) \end{bmatrix} \begin{bmatrix} K_{diff,\,red} & K_{diff,\,green} & K_{diff,\,blue} \\ K_{spec,\,red} & K_{spec,\,green} & K_{spec,\,blue} \end{bmatrix} \\
&= \begin{bmatrix} \underset{\sim}{G}_{diff} & \underset{\sim}{G}_{spec} \end{bmatrix} \begin{bmatrix} \underset{\sim}{K}^T_{diff} \\ \underset{\sim}{K}^T_{spec} \end{bmatrix} \\
&\equiv GK
\end{aligned}
\qquad \textbf{(EQ4)}
$$

where $P(\theta) = \left(\exp\left(-\theta^2/\sigma_\alpha^2\right)\right)/\cos\theta$, and the two vectors $\underset{\sim}{G}_{diff}$ and $\underset{\sim}{G}_{spec}$ represent the intensity values of the diffuse and specular reflection components with respect to the sensor direction $\theta$. The vector $\underset{\sim}{K}_{diff}$ represents the diffuse reflection color vector. The vector $\underset{\sim}{K}_{spec}$ represents the specular reflection color vector. We call the two matrices $G$ and $K$, the *geometry matrix* and the *color matrix,* respectively.

Suppose we have an estimation of the color matrix $K$. Then, the two reflection components represented by the geometry matrix $G$ are obtained by projecting the observed reflection stored in $M$ onto the two color vectors $\underset{\sim}{K}_{diff}$ and $\underset{\sim}{K}_{spec}$.

$$G = MK^+ \qquad \textbf{(EQ5)}$$

where $K^+$ is a $3 \times 2$ pseudoinverse matrix of the color matrix $K$.

The derivation shown above is based on the assumption that the color matrix $K$ is known. In our experiments, the specular reflection color vector $\underset{\sim}{K}_{spec}$ is directly measured by using a standard color chart. Therefore, only the diffuse color vector $\underset{\sim}{K}_{diff}$ is unknown. The method to estimate the diffuse color vector is explained in the following section.

- **Estimation of the diffuse reflection color**

From (EQ1), it can be seen that the distribution of the specular reflection component is limited to a fixed angle, depending on $\sigma_\alpha$. Therefore, if two vectors, $\underset{\sim}{w}_i = \begin{bmatrix} I_{Ri} & I_{Gi} & I_{Bi} \end{bmatrix}^T$

($i = 1, 2$) are sampled on the $\theta$ axis at large enough interval, at least one of these vectors will be equal to the color vector of the diffuse reflection component $\underset{\sim}{K}^T_{diff}$. This vector has no specular reflection component. The desired color vector of the diffuse reflection component $\underset{\sim}{K}^T_{diff}$ is the vector $\underset{\sim}{w}_i$ which subtends the largest angle with respect to the vector $\underset{\sim}{K}^T_{spec}$. The angle between the two color vectors can be calculated as:

$$\beta = \operatorname{acos} \frac{\underset{\sim}{K}^T_{spec} \cdot \underset{\sim}{w}_i}{\left|\underset{\sim}{K}^T_{spec}\right| \left|\underset{\sim}{w}_i\right|} \tag{EQ6}$$

Once we get the color matrix $K$, the geometry matrix $G$ can be calculated from (EQ5). Then, each of the diffuse and specular reflection components are given as:

$$M_{diff} = \underset{\sim}{G}_{diff} \underset{\sim}{K}^T_{diff} \tag{EQ7}$$

$$M_{spec} = \underset{\sim}{G}_{spec} \underset{\sim}{K}^T_{spec} \tag{EQ8}$$

## 3.3 Reflectance parameter estimation for segmented regions

In the previous section, the method to separate the two reflection components from a sequence of observed colors of each triangular patch was described. In this section, we will discuss how to estimate parameters of the reflectance model for the triangular patch by using the separated reflection components.

By applying the separation algorithm that was explained in the previous section, we obtain a sequence of the diffuse reflection component and a sequence of the specular reflection component for each triangular patch. That makes it possible to estimate reflectance parameters of the reflection model (EQ1) separately for the two reflection components. The parameter estimation is performed for each triangular patch one by one. As (EQ1) shows, the reflectance model is a function of the angle between the surface normal and the viewing direction $\theta$. Therefore, for estimating reflectance parameters: $K_{diff,\,m}$, $K_{spec,\,m}$, and $\sigma_\alpha$, the angle $\theta$ has to be computed as the rotary table rotates. Since the projection transformation matrix is already given and the object orientation is known in the world coordinate system, it is straightforward to compute a surface normal vector and a viewing direction vector (or a illumination vector) at a center of each triangular patch. Thus, the angle $\theta$ between the surface normal and the viewing direction vector can be computed. After the angle $\theta$ is computed, the reflectance parameters for the diffuse reflection component ($K_{diff,\,m}$) and the specular reflection component ($K_{spec,\,m}$ and $\sigma_\alpha$) are estimated separately by the Levenberg-Marquardt method [16]. In our experiment, the camera output is calibrated so that the specular reflection color has the same value from the three color channels. Therefore, only one color band is used to estimate $K_{spec}$ in our experiment.

By repeating the estimation procedure for all triangular patches, we can estimate the diffuse reflection component parameters for all triangular patches if those patches are illuminated in one or more frames of the image sequence. On the other hand, the specular reflection component can be observed only in a limited viewing direction. Due to this fact, the specular reflection component can be observed only in a small subset of all triangular patches. We cannot estimate the specular reflection component parameters for those patches in which the specular reflection component is not observed. Even if the specular reflection component is observed, the parameter estimation can become unreliable if the specular reflection is not sufficiently strong. To avoid that, we can increase the number of sampled object orientations and take more color images. However, that still cannot guarantee that all triangular patches show the specular reflection component. Taking more color images may not be practical since more sampled images require more measurement time and data processing time.

For the above reasons, we decided to assign the specular reflection component parameters based on region segmentation. In our experiments, it is assumed that the object surface can be segmented into a finite number of regions which have uniform diffuse color, and all triangular patches within each region have the same specular reflection component parameters. If the region segmentation cannot be performed correctly (e.g. fine texture on the object surface), the segmentation can be done by other measures such as uniform surface normal directions, depending on the type of target objects. By using the segmentation algorithm, the specular reflection parameters of each region can be estimated from triangular patches with strong specularity. The estimated parameters are assigned to the rest of patches in the region. The triangular patches with strong specularity can be easily selected after the reflectance component separation explained in the section 3.2. The limitation of this approach is that the specular reflection parameters for a region cannot be estimated if no specularity is observed in the region. In that case, the specular reflection parameters of neighboring regions can be assigned to the region as an approximation. It is important to note that the segmentation and parameter estimation are used only for the specular reflection component. The diffuse reflection component parameter are estimated locally regardless of specularity.

After reflectance parameters are estimated for all triangular patches, we have the object shape as a collection of triangular patches and reflectance parameters for those patches. This information can be used for synthesizing computer graphics images with physically correct reflection. Some examples of synthesized images will be shown in the section 4.7.

# 4 Experimental results

## 4.1 Experimental setup

In the previous sections, we described the method to obtain shape and reflectance information from multiple range images and color images. The method includes three steps: 1. merging multiple triangular surface patches into one patch to generate an object shape model, 2. separating the two fundamental reflection components from a sequence of color images, and 3. estimating the reflection model parameters from the separated reflection components. We applied the method to actual range and color images taken in a laboratory setup, in order to demonstrate the feasibility of the proposed method. A SONY CCD color video camera module model XC-711 is used to take color images in our experiments. A light stripe range finder with a liquid crystal shutter is used for taking range images. The same color camera is used to take images in the range finder. This guarantees correspondence between the range images and the color images at each pixel. The target object used in our experiment is a plastic dinosaur with an approximate height of $170mm$. The object is painted in several colors, and each painted surface region appears to have a uniform color. The object is located on a rotary table whose orientation can be controlled by a computer. Multiple range and color images of the object are taken for different object orientations. A single xenon lamp whose diameter is approximately 10mm is used as a point light source. The light source is located close by the camera, and the light source direction is considered to be the same as the viewing direction. The camera and light source locations are fixed in our experiment. The approximate distance between the object and the camera is $2m$. Our experimental setup is illustrated in Figure 1.

The range finder is calibrated to obtain the $4 \times 3$ projection transformation matrix between the world coordinate system and the image coordinate system. The matrix is used for mapping the color images onto the recovered object shape. The location and orientation of the rotary table in the world coordinate system is also measured by using a calibration box and the range finder. As a result, the direction and location of the rotation axis in the world coordinate system are known. They are used for projecting the color images onto the recovered object shape as described in the section 2.2. The color video camera is calibrated by using a standard color chart to ensure linear response from all three color bands. The color chart is also used for measuring the light source color. Therefore, the illumination color is assumed to be known in our experiment.

## 4.2 Measurement

Range images and color images of the target object are taken by using the experimental setup described in the previous section. The object is placed on the rotary table, and range images and color images are captured as the object rotates on the table. In our experiment, range images are captured for every $45°$, and color images are obtained for every $3°$. In total, 8 range images and 120 color images are digitized. The reason why we need more color images than range images is because fine sampling is necessary to capture the specular reflection distribution correctly. On the other hand, the range images are used only for recovering the object shape, and it does not require fine sampling. The small number of images are sufficient to observe the object shape entirely. Two frames of the input range images are shown as triangular surface patches in Figure 2. Color Figure 1 shows the sequence of input color images. Six frames out of 120 are shown as examples.

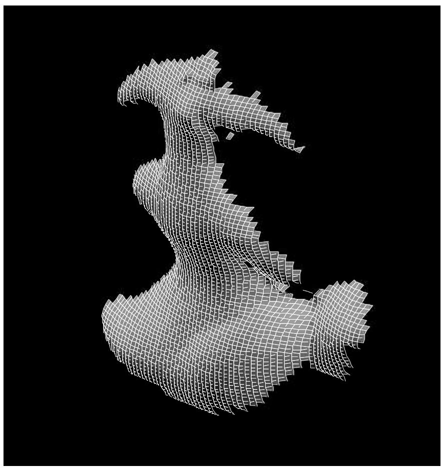

frame 0: object orientation = 0°

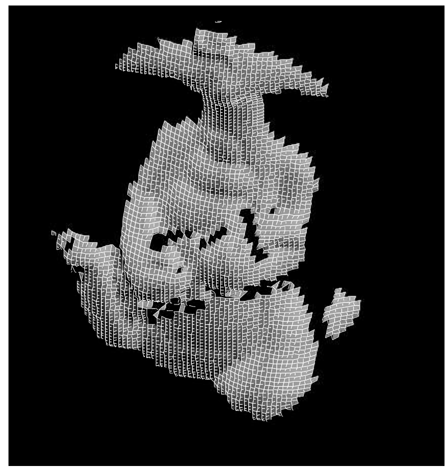

frame 4: object orientation = 180°

**Figure 2 Input range data: 2 out of 8 frames are shown here.**

## 4.3 Shape recovery

The zipper system [23] was used for merging eight triangular surface meshes created from the input range images. The recovered object shape is shown in Figure 3. The object shape consists of 9943 triangular patches. In the process of merging surface meshes, the object shape was manually edited to remove noticeable defects such as holes and spikes. The manual edit will be unnecessary if more range images are used.

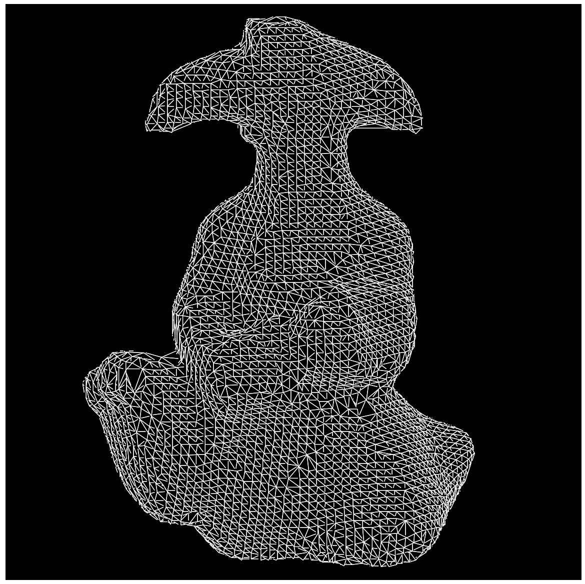

**Figure 3 Recovered object shape**

## 4.4 View mapping

After the object shape is generated from the range images, the sequence of input color images are mapped onto the recovered object shape as described in the section 2.2. The result of the color image mapping is illustrated in Color Figure 2. Six frames are shown as examples here.

Based on the image mapping onto the recovered object shape, a sequence of observed colors is determined at each triangular patch of the object shape as explained in the section 2.2. The observed color is not defined if the triangular patch is not visible from the camera. In this case, the observed color is set to zero. Figure 4 illustrates a typical observed color sequence at a triangular patch with strong specularity. The specular reflection component can be observed strongly near image frame 67. When the specular reflection component exists, the output color intensity is a linear combination of the diffuse reflection component and the specular reflection component. The two reflection components are separated by using the algorithm explained in the section 3.2, and the separation result will be shown in the next section. The intensities are set to zero before the image frame 39 and after the image frame 92 because the triangular patch is not visible from the camera due to occlusion. Another example with weak specularity is shown in Figure 5. In the example, the observed specular reflection is relatively small compared to the diffuse reflection component. As a result, estimating reflectance parameters for both the diffuse and specular reflection components together could be sensitive to various disturbances such as image noise. That is why the reflection component separation is introduced in prior to parameter estimation in our analysis. By separating the two reflection components based on color, reflectance parameters can be estimated separately in a robust manner.

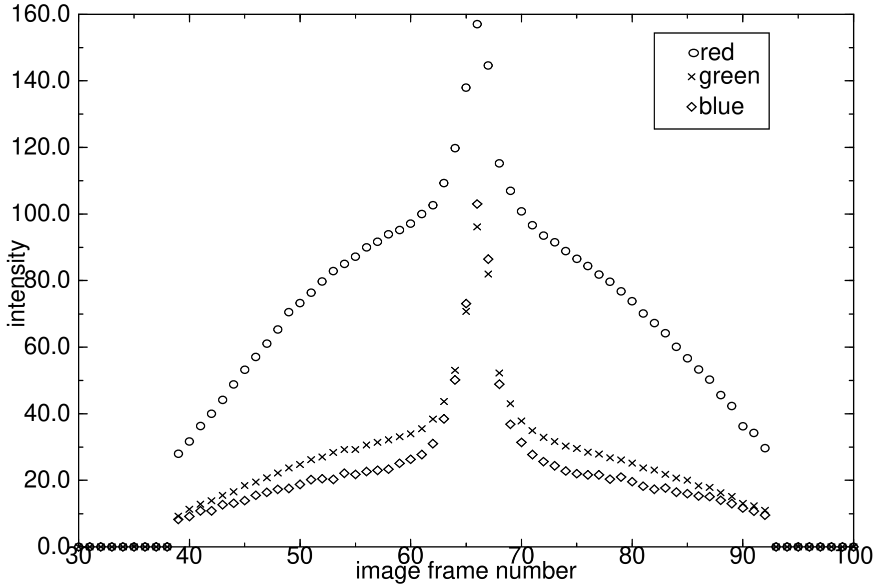


**Figure 4 intensity change with strong specularity**

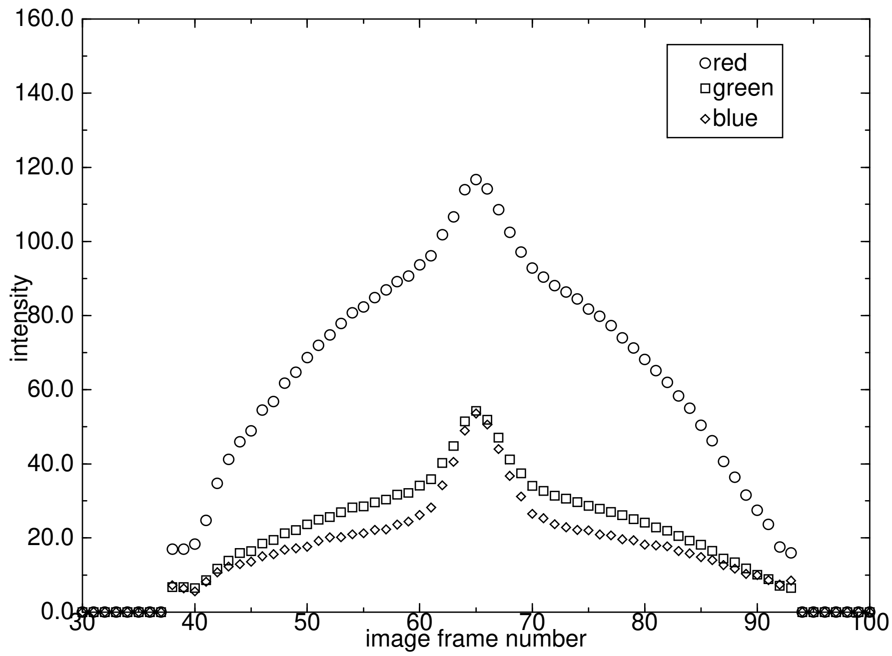


**Figure 5 intensity change with little specularity**

## 4.5 Reflection component separation

The algorithm to separate the diffuse and specular reflection components, described in the section 3.2, was applied to the observed color sequence at each triangular patch. The red, green, and blue intensities of the observed color sequence are stored in the matrix $M$ as its columns

(EQ4). Then, the matrix $G$ is computed from the matrix $M$ and the matrix $K$ which is estimated as described in the section 3.2.1. Finally, the diffuse and specular reflection components are given as shown in (EQ7) and (EQ8). This reflection component separation is repeated for all triangular patches of the object. Some of the separation results are shown in Figure 6 and Figure 7. Figure 6 shows the separated reflection components with strong specularity. The measured color sequence is shown in Figure 4 in the previous section. Another example of the reflection component separation is given in Figure 7. In that case, the specular reflection component is relatively small compared to the diffuse reflection component. That example indicates that the separation algorithm can be applied robustly even if the specularity is not observed strongly. After the reflection component separation, reflectance parameters can be estimated separately. The result of parameter estimation will be shown in the section 4.6.

The separated reflection components at all triangular patches of a particular image frame can be used to generate the diffuse reflection image and the specular reflection image. The result of the diffuse and specular reflection images are shown in Color Figure 3 and Color Figure 4. Image frame 0 and 60 are used to generate Color Figure 3 and Color Figure 4, respectively.

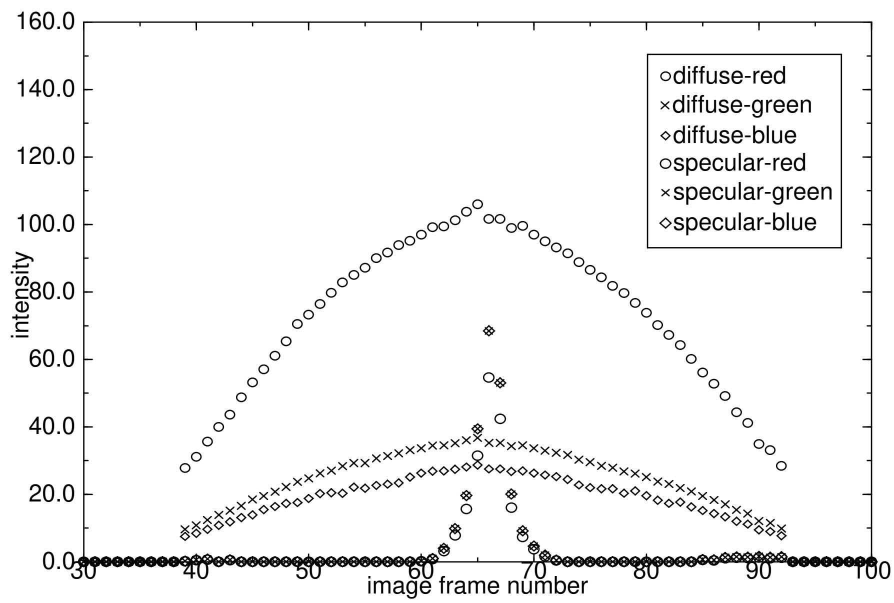


**Figure 6 separated reflection components with strong specularity**

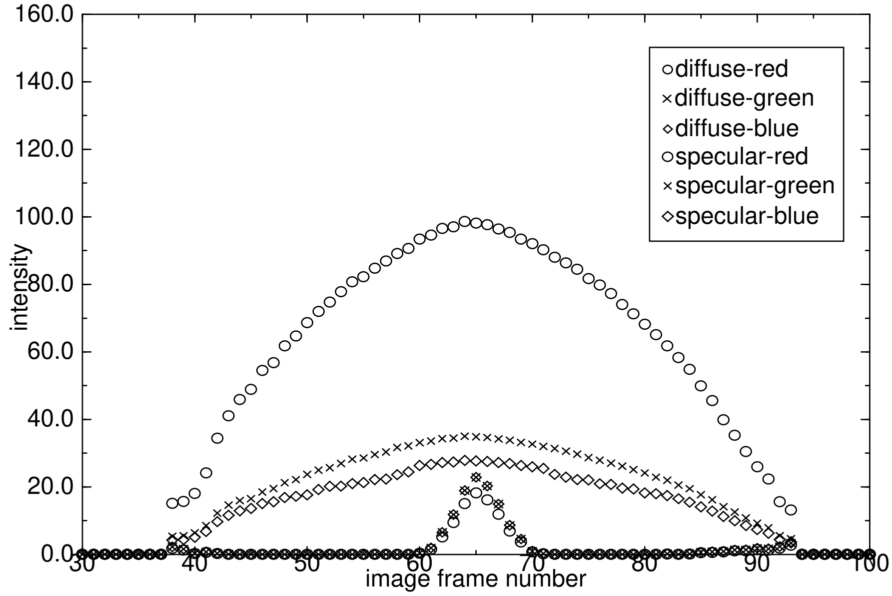


**Figure 7 separated reflection component with little specularity**

## 4.6 Reflectance parameter estimation for segmented regions

By using the separated diffuse reflection components of all triangular patches, the object surface was segmented based on the hue of the diffuse reflection components, as explained in the section 3.3. The result of the region segmentation is shown in Figure 8 where segmented regions are represented as grey level. For estimating specular reflection component parameters, ten triangular patches with the largest specular reflection component are selected for each of the segmented regions. Then, the specular reflection component parameters of the reflection model (EQ1) are estimated by the Levenberg-Marquardt method for each of the ten selected triangular patches. Finally, the average of the estimated parameters of the selected triangular patches is used as the specular reflection component parameters of the segmented region. The estimated specular reflection parameters are assigned to all triangular patches within the segmented region. In our experiments, the four largest segmented regions were used for specular reflection parameter estimation, and the rest of small regions were not used. The small regions were found to be located near or at the boundaries of the large regions. Hence, a surface normal of a triangular patch does not necessarily represent a surface normal of the object surface at the location. That causes the parameter estimation to be inaccurate. Therefore, those small regions are assumed to have the same specular reflection properties as the large regions in our analysis. The result of the estimated specular reflection component parameters is shown in Table 1.

Unlike the specular reflection parameter estimation, parameters of the diffuse reflection component are estimated for each triangular patch individually. That is because the diffuse reflection component at the triangular patch is guaranteed to be observed as long as the patch is illuminated and not occluded from the viewing direction. The result of the diffuse reflection component parameter estimation will be shown in the next section as synthesized images of the object.

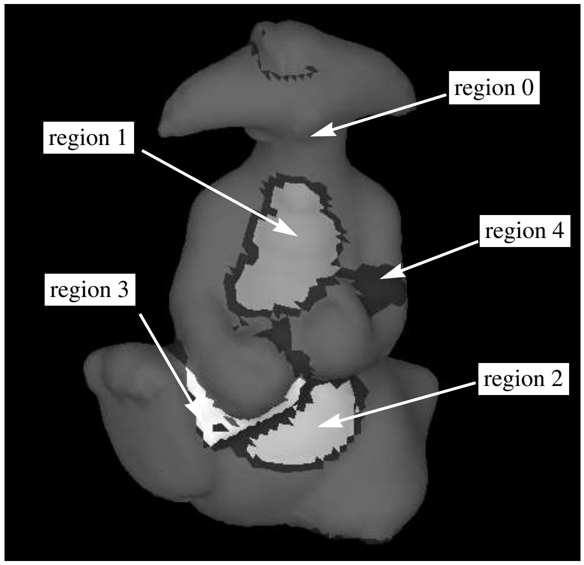


**Figure 8 Segmentation result (grey levels represent regions)**

**Table 1 estimated parameters of the specular reflection component**

| region # | $K_{spec}$ | $\sigma_{\alpha}$ |
|---|---|---|
| 0 | 134.58 | 0.091 |
| 1 | 111.32 | 0.119 |
| 2 | 38.86 | 0.147 |
| 3 | 39.87 | 0.177 |

## 4.7 Synthesized images with correct reflection

By using the recovered object shape and reflection model parameters, images of the object under arbitrary illumination conditions can be generated. In this section, some of the images are shown to demonstrate the feasibility of the proposed method to produce highly realistic images. Point light sources located far from the object are used for generating images. Color Figure 5 shows the object illuminated from the left side. The arrow in the image represents the illumination direction. It is important to see that region 2 shows less specularity than region 0 and region 1. (See Figure 8 for region numbers.) In addition, the specular reflection is widely distributed in region 2 because region 2 has a large reflectance parameter $\sigma_{\alpha}$. Another example image with a different illumination direction is shown in Color Figure 6. The object is illuminated by incoming light from the upper right side in the image. Color Figure 7 shows the object illuminated by two light sources. In the example, highlights on the object surface appear to be a combination of highlights shown in Color Figure 5 and Color Figure 6.

# 5 Conclusion

We have studied an approach for creating a three dimensional object model with physically correct reflectance properties by observing a real object. The Lambertian model and the Torrance-Sparrow reflection model are used as the basic reflectance model in our analysis. The object is located on a rotary table, and a sequence of range and color images are taken as the object rotates. First, the object shape is recovered from a range image sequence as a collection of triangular patches. Then, a sequence of input color images are mapped onto the recovered object shape to determine an observed color sequence at each triangular patch individually. The observed color sequence is separated into the diffuse and specular reflection components. Finally, parameters of the Lambertian model and the Torrance-Sparrow model are estimated separately at each of triangular patches. By using the recovered object shape and estimated reflectance parameters associated with each triangular patch, highly realistic images of the real object can be synthesized under arbitrary illumination conditions. The proposed approach has been applied to real range and color images of a plastic object, and the effectiveness of the proposed approach has been successfully demonstrated by showing synthesized images of the object under different illumination conditions.

# Appendix A Simplified Torrance-Sparrow model

In our work, the Torrance-Sparrow model [22] is used for representing the specular lobe reflection component. The model describes single reflection of incident light rays by rough surfaces. This model is reported to be valid when the wavelength of light is much smaller than the roughness of the surface [22], which is always true in our experiments. The surface is modelled as a collection of planer micro-facets which are perfectly smooth and reflect light rays as perfect specular reflectors. The geometry for the Torrance-Sparrow model is shown in Figure 9. The surface area $dA_s$ is located at the center of the coordinate system. An incoming light beam lies in the $X-Z$ plane and is incident on the surface at an angle $\theta_i$. The radiance and solid angle of the light source are represented as $L_i$ and $d\omega_i$, respectively.

In the Torrance-Sparrow model, the micro-facet slopes are assumed to be normally distributed. Additionally, the distribution is assumed to be symmetric around the mean surface normal $\vec{n}$. The distribution is represented by a one-dimensional normal distribution:

$$\rho_\alpha(\alpha) = ce^{-\frac{\alpha^2}{2\sigma_\alpha^2}} \quad \textbf{(EQ9)}$$

where $c$ is a constant, and the facet slope $\alpha$ has mean value $\langle\alpha\rangle = 0$ and standard deviation $\sigma_\alpha$.

In the geometry shown in Figure 9, only planar micro-facets having normal vectors within the solid angle $d\omega'$ can reflect incoming light flux specularly. The number of facets per unit area of the surface that are oriented within the solid angle $d\omega'$ is equal to $\rho_\alpha(\alpha)\,d\omega'$. Hence, considering the area of each facet $a_f$ and the area of the illuminated surface $dA_s$, the incoming flux on the set of reflecting facets is determined as:

$$d^2\Phi_i = L_i d\omega_i (a_f \rho_\alpha(\alpha)\,d\omega' dA_s)\cos\theta_i' \quad \textbf{(EQ10)}$$

The Torrance and Sparrow model considers two terms to determine what portion of the incoming flux is reflected as outgoing flux. One term is the Fresnel reflection coefficient, $F(\theta_i', \eta', \lambda)$ where $\eta'$ is the refractive index of the material, and $\lambda$ is the wave length of the incoming light. Its value for a perfect mirror-like surface depends on wavelength, incident angle and material. The other term is called the geometric attenuation factor, and it is represented as $G(\theta_i, \theta_r, \phi_r)$. It accounts for the fact that at large incidence angles light incoming to a facet may be shadowed by adjacent surface irregularities, and outgoing light along the viewing direction that grazes the surface may be masked or interrupted in its passage to the viewer. Considering those two factors, the flux $d^2\Phi_r$ reflected into the solid angle $d\omega_r$ is determined as:

$$d^2\Phi_r = F(\theta_i', \eta', \lambda)\, G(\theta_i, \theta_r, \phi_r)\, d^2\Phi_i \quad \textbf{(EQ11)}$$

The radiance of reflected light is defined as:

$$dL_{spec,r} = \frac{d^2\Phi_r}{d\omega_r dA_s \cos\theta_r} \quad \textbf{(EQ12)}$$

Substituting (EQ10) and (EQ11) into(EQ12), we obtain:

$$dL_{spec,r} = \frac{F(\theta_i', \eta', \lambda)\, G(\theta_i, \theta_r, \phi_r)\, L_i d\omega_i\, (a_f \rho_\alpha(\alpha)\, d\omega' dA_s) \cos\theta_i'}{d\omega_r dA_s \cos\theta_r} \quad \textbf{(EQ13)}$$

Since only facets with normals that lie within the solid angle $d\omega'$ can reflect light into the solid angle $d\omega_r$, the those two solid angles are related as:

$$d\omega' = \frac{d\omega_r}{4\cos\theta_i'} \quad \textbf{(EQ14)}$$

Substituting (EQ14) into (EQ13), surface radiance of the surface $dA_s$ given by the specular reflection component is represented as:

$$dL_{spec,r} = \frac{c a_f F(\theta_i', \eta', \lambda)\, G(\theta_i, \theta_r, \phi_r)}{4} \frac{L_i d\omega_i}{\cos\theta_r} e^{-\frac{\alpha^2}{2\sigma_\alpha^2}} \quad \textbf{(EQ15)}$$

As stated above, the Fresnel coefficient $F(\theta_i', \eta', \lambda)$ and the geometrical attenuation factor $G(\theta_i, \theta_r, \phi_r)$ depend on the illumination and viewing geometry. In our experiments, the geometry is simplified because the viewing direction and the illumination direction always coincide. The simplified geometry is shown in Figure 10. Substituting $\theta_i = \theta_r = \alpha$, $\theta_i' = 0$, and $\phi_r = \pi$, (EQ15) is simplified to:

$$dL_{spec,r} = \frac{c a_f F(0, \eta', \lambda)\, G(\theta_i, \theta_i, \pi)}{4} \frac{L_i d\omega_i}{\cos\theta_i} e^{-\frac{\theta_i^2}{2\sigma_\alpha^2}} \quad \textbf{(EQ16)}$$

It is observed that the geometrical attenuation factor $G$ equals unity for angles of incidence not near the grazing angle. Since that is not the case in our experiment, the geometrical attenuation factor $G$ is assumed to be constant in our analysis. The Fresnel coefficient can be regarded as a function of the wave length $\lambda$ because the local angle of incidence $\theta_i'$ is always equal to $0$. Finally, the surface radiance of the specular reflection component in our experiments is represented as:

$$dL_{spec,\,r} = \frac{ca_f F(\lambda)\, G}{4} \frac{L_i d\omega_i}{\cos\theta_i} e^{-\frac{\theta_i^2}{2\sigma_\alpha^2}} \quad \textbf{(EQ17)}$$

The dichromatic reflection model [20] predicts that a reflection mechanism is modelled as a linear combination of two reflection components: the diffuse reflection component and the specular reflection component. According to the dichromatic reflection model, the reflection model used in this paper is represented as a combination of the Lambertian model and (EQ17):

$$dL_r = \left\{ k_{diff}(\lambda) \cos\theta_i + \frac{k_{spec}(\lambda)}{\cos\theta_i} e^{-\frac{\theta_i^2}{2\sigma_\alpha^2}} \right\} L_i d\omega_i \quad \textbf{(EQ18)}$$

where $k_{diff}(\lambda)$ represents the ratio of the radiance to the irradiance of the diffuse reflection, and $k_{spec}(\lambda) = ca_f F(\lambda)\, G/4$. That expression is integrated in the case of a collimated light source to produce:

$$L_r = \int_{\omega_i} dL_r = k_{diff}(\lambda)\, s(\lambda) \cos\theta + \frac{k_{spec}(\lambda)\, s(\lambda)}{\cos\theta} e^{-\frac{\theta^2}{2\sigma_\alpha^2}} \quad \textbf{(EQ19)}$$

where $s(\lambda)$ is the surface irradiance on a plane perpendicular to the light source direction.

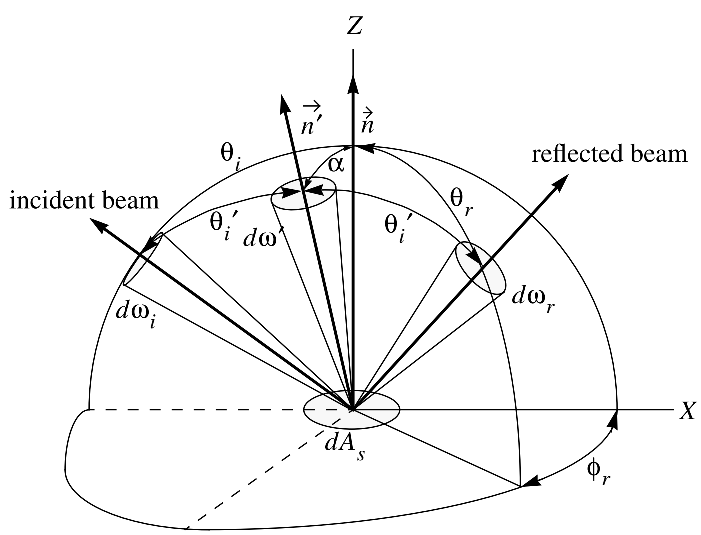


**Figure 9 Geometry for Torrance-Sparrow model [22]**

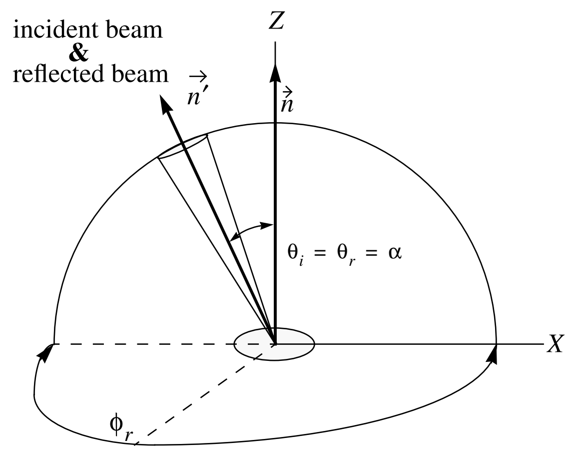


**Figure 10 Simplified geometry**

# Appendix B Image formation model

If the object distance is much larger than the focal length and the diameter of the entrance pupil of the imaging system, it can be shown that the image irradiance $E_p$ is proportional to scene radiance $L_r$. It is given as:

$$E_p = L_r \frac{\pi}{4}\left(\frac{d}{f}\right)^2 \cos^4\gamma \qquad \textbf{(EQ20)}$$

where $d$ is the diameter of a lens, $f$ is the focal length of the lens, and $\gamma$ is the angle between the optical axis and the line of sight [8]. In our experiments, changes of those three parameters $d$, $f$, and $\gamma$ are assumed to be relatively small. Therefore, (EQ20) can be simply given as:

$$E_p = gL_r \qquad \textbf{(EQ21)}$$

where $g = \frac{\pi}{4}\left(\frac{d}{f}\right)^2 \cos^4\gamma$. Combining (EQ19) and (EQ21), we have:

$$E_p = gk_{diff}(\lambda)\, s(\lambda) \cos\theta + \frac{gk_{spec}(\lambda)\, s(\lambda)}{\cos\theta} e^{-\frac{\theta^2}{2\sigma_\alpha^2}} \qquad \textbf{(EQ22)}$$

Now let $\tau_m(\lambda)$, $m = (red, green, blue)$ be the spectral responsivity of the color camera in red, green and blue bands. Then, the output from the color camera in each band can be expressed as:

$$I_m = \int_\lambda \tau_m(\lambda)\, E_p(\lambda)\, d\lambda \qquad \textbf{(EQ23)}$$

This equation can be simplified as:

$$I_m = K_{diff,\, m} \cos\theta + K_{spec,\, m} \frac{1}{\cos\theta} e^{-\frac{\theta^2}{2\sigma_\alpha^2}} \qquad \textbf{(EQ24)}$$

where

$$K_{diff,\, m} = g\int_\lambda \tau_m(\lambda)\, k_{\mathrm{diff}}(\lambda)\, s(\lambda)\, d\lambda$$

$$K_{spec,\, m} = g\int_\lambda \tau_m(\lambda)\, k_{\mathrm{spec}}(\lambda)\, s(\lambda)\, d\lambda \qquad \textbf{(EQ25)}$$

# Color figures

frame#=0

frame#=20

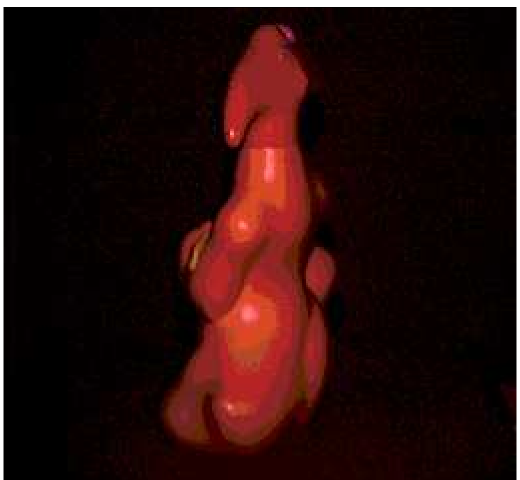

frame#=40

frame#=60

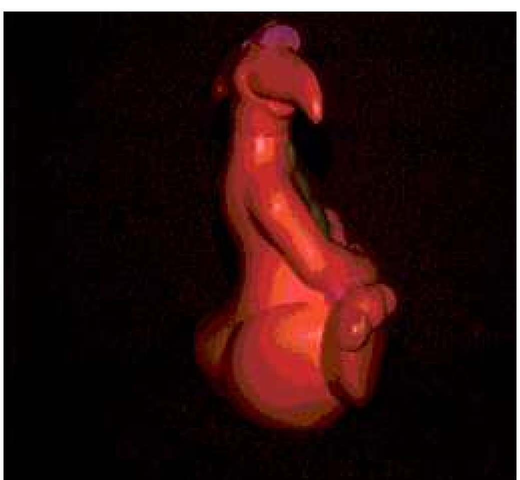

frame#=80

frame#=100

**Color Figure 1  Input color images**

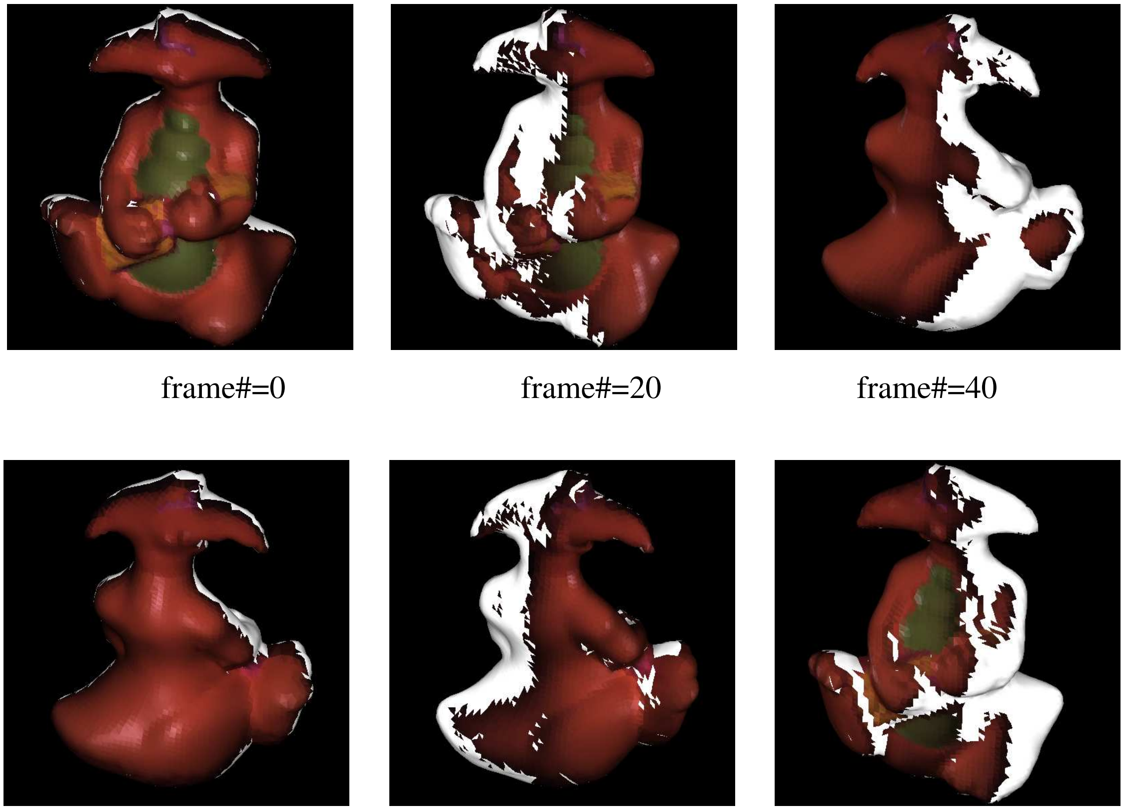

frame#=0 frame#=20 frame#=40

frame#=60 frame#=80 frame#=100

**Color Figure 2  View mapping result**

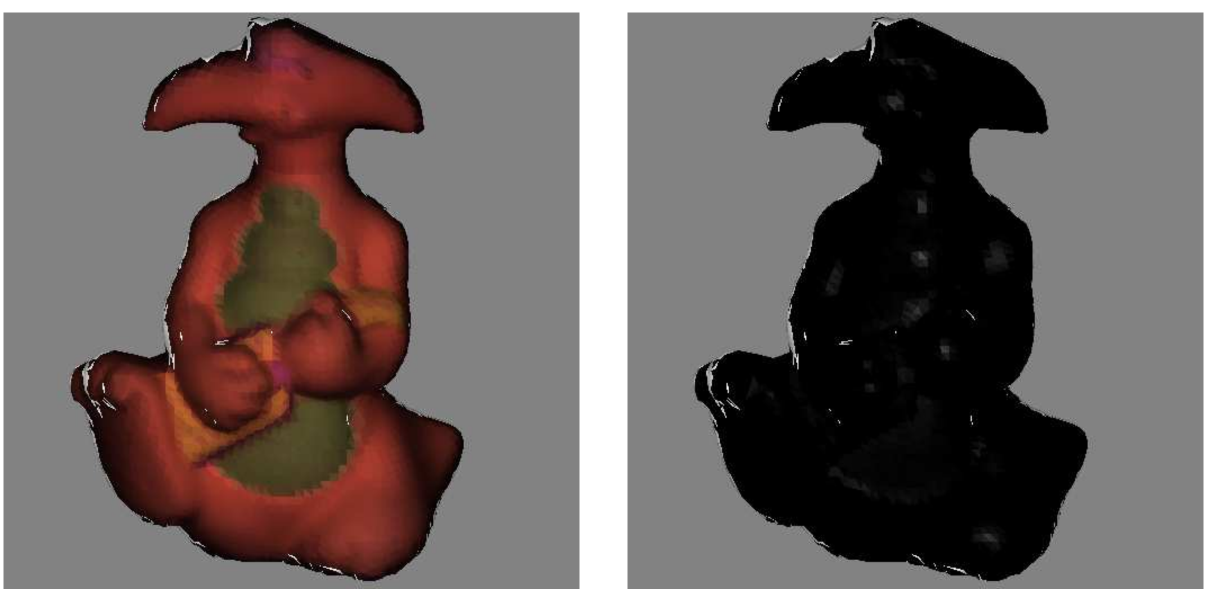

**Color Figure 3  diffuse image and specular image: example 1**

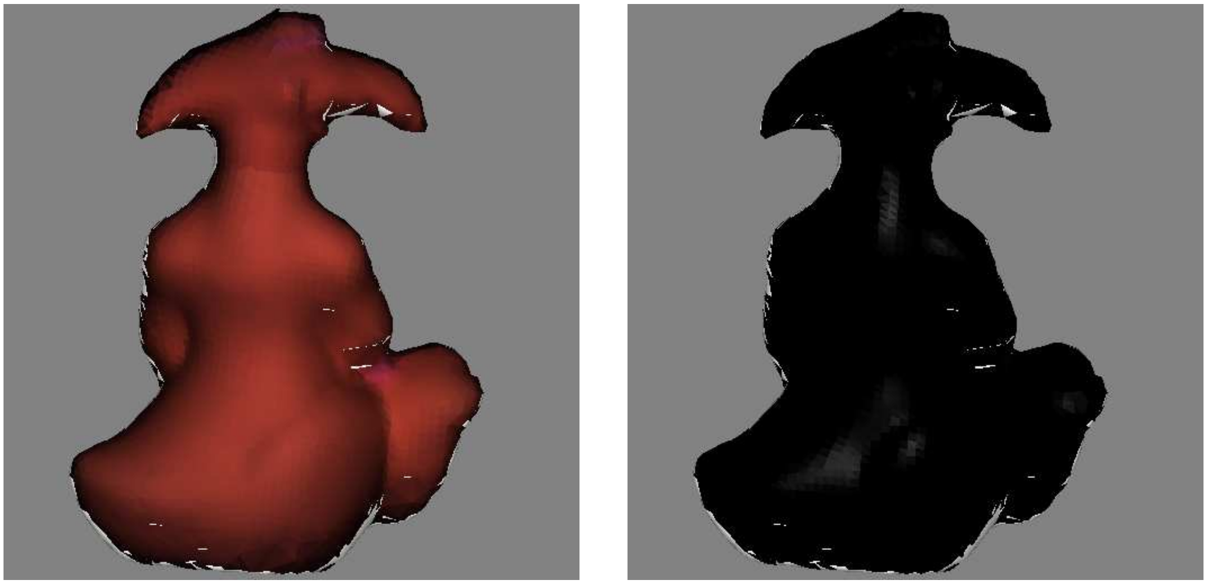

Color Figure 4  diffuse image and specular image: example 2

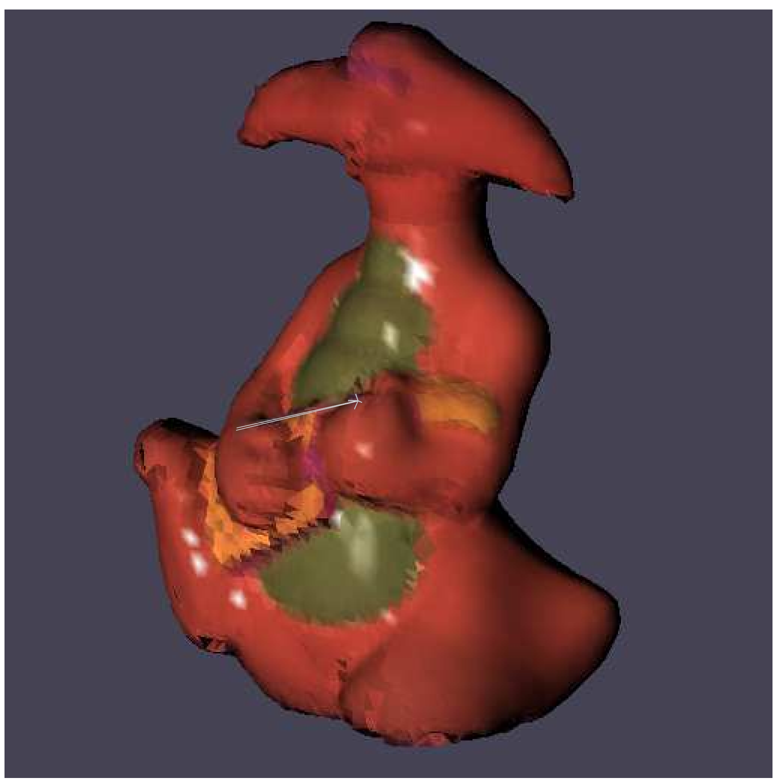

Color Figure 5  Synthesized image 1

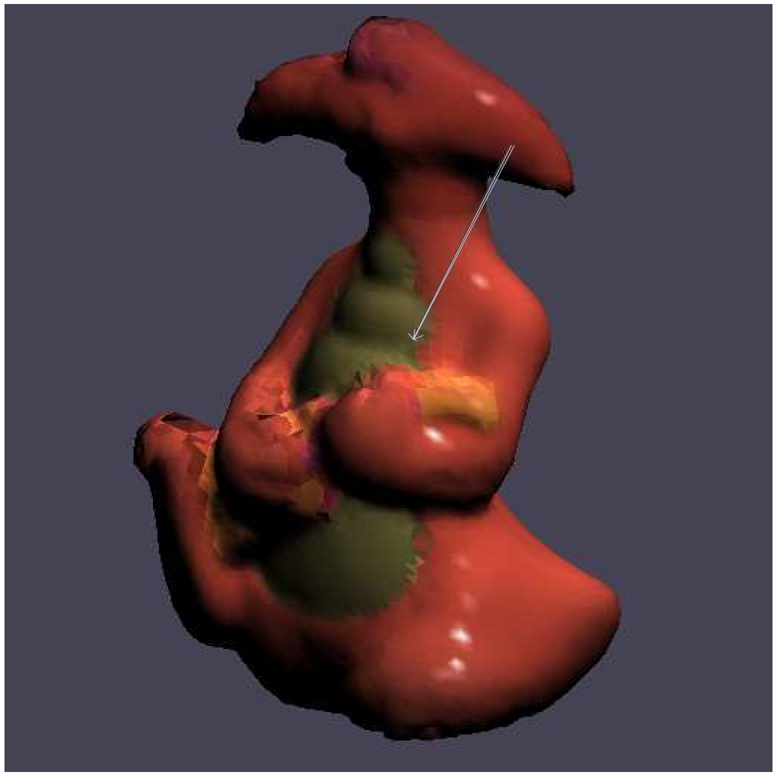

**Color Figure 6 Synthesized image 2**

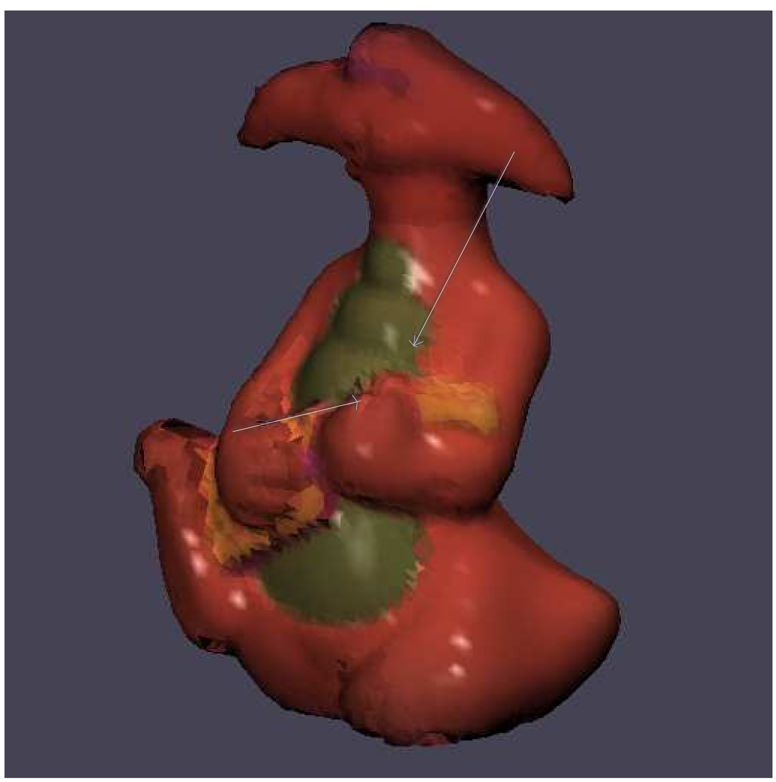

**Color Figure 7 Synthesized image 3**

# Acknowledgments

The authors are thankful to Fred Solomon for his valuable comments on the manuscript.

# References


[1] R. Baribeau, M. Rioux and G. Godin, "Color reflectance modeling using a polychromatic laser range sensor," *IEEE Trans. Pattern Analysis and Machine Intelligence*, Vol. 14, No. 2, February 1992.

[2] P. J. Besl and N. D. McKay, "A method of registration of 3-D shapes," *IEEE Trans. on Pattern Analysis and Machine Intelligenc*e, Vol. 14, No. 2, pp. 239-256, February 1992.

[3] R. L. Cook and K. E. Torrance, "A reflectance model for computer graphics," *ACM Trans. Graphics*, Vol. 1, No. 1, pp. 7-24, 1982.

[4] H. Delingette, M. Hebert, and K. Ikeuchi, "Object modeling by registration of multiple range images," *Image and Vision Computing*, Vol. 10, No. 3, April 1992.

[5] G. Healey, "Using color for geometry-insensitive segmentation," *Journal of Optical Society of America A*, Vol. 6, No. 6, pp. 920-937, June 1989.

[6] K. Higuchi, M. Hebert and K. Ikeuchi, "Building 3-D models from unregistered range images," Technical Report CMU-CS-93-214, November 1993.

[7] H. Hoppe, T. DeRose and T. Duchamp, "Surface reconstruction from unorganized points," *Computer Graphics* (SIGGRAPH '92), Vol. 26, No. 2, pp. 71-78, July 1992.

[8] B. K. P. Horn and R. W. Sjoberg, "Calculating the reflectance map," *Appl. Opt.* Vol. 18, No. 11, pp. 1770-1779, June 1979.

[9] K. Ikeuchi and K. Sato, "Determining reflectance properties of an object using range and brightness images," *IEEE Trans. Pattern Analysis and Machine Intelligence*, Vol. 13, No. 11, p. 1139-1153, November 1991.

[10] G. Kay and T. Caelli, "Inverting an illumination model from range and intensity maps," *CVGIP: Image Understanding*, Vol. 59, No. 2, pp. 183-201, March 1994.

[11] H. Lee, E. J. Breneman and C. P. Schulte, "Modeling light reflection for computer color vision," *IEEE Trans. Pattern Analysis and Machine Intelligence*, Vol. 12, No. 4, pp. 402-409, 1990.

[12] J. Lu and J. Little, "Reflectance function estimation and shape recovery from image sequence of a rotating object," to be appeared in *International Conference on Computer Vision '95*, June 1995.

[13] S. K. Nayar, K. Ikeuchi and T. Kanade, "Surface reflection: physical and geometrical perspectives," *IEEE Trans. on Pattern Analysis and Machine Intelligence,* Vol. 13, No. 7, pp. 611-634, 1991.

[14] F. E. Nicodemus, J. C. Richmond, J. J. Hsia, I. W. Ginsberg and T. Limperis, "Geometrical considerations and nomenclature for reflectance," NBS Monograph 160, Nat. Bureau Standards, Washington DC, October 1977.

[15] B. Phong, "Illumination for computer-generated pictures," *Comm. ACM*, Vol. 18, No. 6, pp. 311-317, 1975.

[16] W. H. Press, B. P. Flannery, S. A. Teukolsky, and W. T. Vetterling, *Numerical Recipes in C*, Cambridge University Press, New York, 1988.

[17] K. Sato, H. Yamamoto and S. Inokuchi, "Range imaging system utilizing nematic liquid crystal mask," *Proc. International Conference on Computer Vision*, pp. 657-661, 1987.

[18] Y. Sato and K. Ikeuchi, "Temporal-color space analysis of reflection," *Journal of Optical Society of America A*, Vol. 11, No. 11, pp. 2990-3002, November 1994.

[19] Y. Sato and K. Ikeuchi, "Reflectance analysis under solar illumination," to be appeared in *IEEE Physics-Based Modeling and Computer Vision Workshop*, June 1995.

[20] S. Shafer, "Using color to separate reflection components," *COLOR Res. Applications*, Vol. 10, No. 4, pp. 210-218, 1985.

[21] T. M. Strat, "Recovering the camera parameters from a transformation matrix," *Proc. DARPA Image Understanding Workshop*, pp. 264-271, October 1984.

[22] K. E. Torrance and E. M. Sparrow, "Theory for off-specular reflection from roughened surfaces," *Journal of Optical Society of America*, Vol. 57, pp. 1105-1114, 1967.

[23] G. Turk and M. Levoy, "Zippered polygon meshes from range images," *Computer Graphics* (SIGGRAPH '94), pp. 311-318, July, 1994.

[24] G. J. Ward, "Measuring and modeling anisotropic reflection," *Computer Graphics* (SIGGRAPH '92), Vol. 26, No. 2, pp. 265-272, July 1992.